Climatic variability over time scales spanning nine orders of magnitude: Connecting Milankovitch cycles with Hurst-Kolmogorov dynamics

Yannis Markonis* and Demetris Koutsoyiannis

Department of Water Resources and Environmental Engineering, Faculty of Civil Engineering, National Technical University of Athens, Heroon Polytechneiou 5, GR 157 80 Zographou, Greece

*Corresponding author: imarkonis@itia.ntua.gr – tel.: +30 210 7722838

Corrected preprint of a paper published in *Surveys in Geophysics* (with corrections marked)

(doi: 10.1007/s10712-012-9208-9; date of original submission January 2012)

Abstract We overview studies of the natural variability of past climate, as seen from available proxy information, and its attribution to deterministic or stochastic controls. Furthermore, we characterize this variability over the widest possible range of scales that the available information allows and we try to connect the deterministic Milankovitch cycles with the Hurst-Kolmogorov (HK) stochastic dynamics. To this aim, we analyze two instrumental series of global temperature and eight proxy series with varying lengths from 2 thousand to 500 million years. In our analysis we use a simple tool, the climacogram, which is the logarithmic plot of standard deviation versus time scale, and its slope can be used to identify the presence of HK dynamics. By superimposing the climacograms of the different series we obtain an impressive overview of the variability for time scales spanning almost 9 orders of magnitude—from 1 month to 50 million years. An overall climacogram slope of –0.08 supports the presence of HK dynamics with Hurst coefficient of at least 0.92. The orbital forcing (Milankovitch cycles) is also evident in the combined climacogram at time scales between 10 and 100 thousand years. While orbital forcing favours predictability at the scales it acts, the overview of climate variability at all scales suggests a big picture of irregular change and uncertainty of Earth's climate.

Keywords: Hurst-Kolmogorov dynamics, climate variability, Milankovitch theory, paleoclimate, long term persistence, climate reconstructions

1 Introduction

If you thought before science was certain — well, that is just an error on your part.

Richard Feynman, The Character of Physical Law (1994 p. 71).

In the first half of 19th century, geologic evidence indicated that at least one glacial period existed in Earth's geological history (Agassiz 1840; from Imbrie 1982). Some decades later it became clear that during the Pleistocene (2 588 000 – 12 000 years before present time—BP), there were many glacial periods, known also as ice ages, followed by shorter interglacials, such as the one we experience since the onset of human civilization. Ice age lengths ranged from 35–45 thousand years in early Pleistocene to 90–120 thousand years in the last million years. During glacial periods, continental glaciers enlarged in length and volume, reaching the 40th parallel in some regions of the northern hemisphere, while similar phenomena have been identified in the southern hemisphere, too. Milankovitch (1941) provided an explanation for the ice ages based on Earth's orbit variations, which was confirmed after some years by the first temperature reconstructions.

It is now well known that succession of glaciation and deglaciation periods has not occurred all the time, but only in large periods defining an 'icehouse climate', such as the current (Pliocene-Quaternary) icehouse period that started about 2.5 million years ago, as well as the Ordovician and the Carboniferous icehouse periods each of which lasted 50–100 million years (Crowell and Frakes, 1970). In contrast, the 'hothouse climates' are characterized by warmer temperatures, abundance of carbon dioxide (concentrations up to 20–25 times higher than current), and complete disappearance of polar icecaps and continental glaciers. Recently, cosmic ray flux was proposed as the controlling factor of the transition between these states (Shaviv and Veizer 2003). As underlined by Kirkby (2007), this theory was both disputed (Rahmostorf et al. 2004; Royer et al. 2004) and supported (Wallmann 2004; Gies and Helsel 2005).

Additional findings showed that the climate of the Holocene (the last 12 000 years), earlier regarded static, was characterized by many climatic events, such as 'Little Ice Age', 'Medieval Warm Period', 'Holocene Optimum', '8 200 Holocene Event' and 'Bond Events', deviating from 'normal' conditions for hundreds or thousands of years (Bond et al. 2001). For example, during 'Little Ice Age' (1450–1850) the temperature of the Northern hemisphere was about 0.6°C below 1961–1990 average

(Moberg et al. 2005; Pollack and Smerdon 2004), while the 'Medieval Warm Period' (950–1250), was a period of warm climate in Europe and North America and has been related to other climatic events at various regions around the world (Grove and Switsur 1994), including China (Long et al. 2011), New Zealand (Cook et al. 2002) or even Antarctica (Hass et al. 2008).

The preceding 'Younger Dryas' episode is an even more impressive case of abrupt climate change that has occurred in the relatively recent climatic history. At the end of Pleistocene, when the last ice age ended and the retreat of the glaciers had begun, a rapid fall of temperature led the climatic system back to glacial conditions. The 'Younger Dryas' episode lasted for approximately 1300 years (starting at ~12 800 BP), covered spatially both hemispheres and ended even more suddenly than it emerged when temperature increased regionally up to 15^{o}C in few decades (Alley et al. 1993). Although the cause for this short return to an ice age period is still under debate, it has become clear that it is not associated to a single catastrophic event (such as the release of freshwater from the lake Agassiz in Gulf of Mexico or the impact of a comet) but is rather regarded as an integral part of natural variability (Broecker et al. 2010, Mangerud et al. 2010).

All these relatively recent events cannot be attributed to the Milankovitch cycles, whose periods are much longer (see below). Thus, it is very difficult to attribute the climate variability at multiple time scales (from decades to many millions of years) to specific quantifiable causal mechanisms that would be applicable ubiquitously. A more modest goal, which is the purpose of this study, would be to characterize this variability over the widest possible range of scales that the available evidence allows. Such characterization unavoidably uses stochastic descriptions and tools, but without neglecting the influence of identifiable deterministic forcings, such as the variations in Earth's orbit.

Such stochastic descriptions are related to the natural behaviour discovered by the hydrologist H. E. Hurst at the same period of Milankovitch' discovery. Hurst (1951), motivated by the design of High Aswan Dam in Nile and after studying numerous geophysical records, observed that "*although in random events groups of high or low values do occur, their tendency to occur in natural events is greater. This is the main difference between natural and random events*". In other words, in a natural process (e.g. river flow) events of similar type are more likely to occur in groups (e.g. a series of consecutive low flow years) compared to a purely random process (white noise) where grouping of similar states is less frequent.

Unknowingly to Hurst, A. Kolmogorov had already proposed a stochastic process that described this behaviour a decade earlier (Kolmogorov 1940), although both the process and the natural behaviour became widely known after the works of Mandelbrot and Wallis (1968), Klemes (1974) and Leland et al. (1994, 1995). Over the years, this mathematical process (or variants thereof) has be given many names, such as fractional Gaussian noise (FGN), brown noise, fractional ARIMA process (FARIMA) or self-similar process, while the natural behaviour has been called the Hurst phenomenon, long-range dependence (or memory), long term persistence or scaling behaviour (Koutsoyiannis and Cohn 2008). Here, when referring to the relevant natural behaviour, the stochastic process (definition of which will be given in section 5.1), or the related stochastic dynamics, we prefix them with the term Hurst-Kolmogorov (HK) in order to acknowledge the contribution of the two pioneering researchers.

The HK behaviour, detected in numerous time series, as detailed in section 3 below, indicates fluctuations at different time scales, which may reflect the long term variability of several factors such as solar irradiance, volcanic activity and so forth (Koutsoyiannis and Montanari 2006). The multi-scale fluctuations cannot be described adequately by classical statistics, as the latter assumes independence (or weak dependence) and underestimates the system's uncertainty on long time scales, sometimes by two, or even more, orders of magnitude (Koutsoyiannis and Montanari 2007). This underestimation, which some regard counterintuitive, will be further demonstrated below in section 6. Moreover, traditional stochastic autoregressive (AR) models cannot describe these fluctuations in an adequate way, because the autocorrelation functions of these models decay faster than those of the processes they try to model (Beran 1994).

The study of natural variability of past climate can now be based on a lot of available proxy records, some of which are discussed in section 4 and analysed in subsequent sections of this study. These proxies are free of anthropogenic influences that could allegedly contribute to the observed changes. It is our aim to demonstrate some evidence of the presence of HK dynamics at different time scales (spanning 9 orders of magnitude). We also examine the coexistence of deterministic controls (due to orbital forcing) and stochastic dynamics, and try to identify possible connections between this stochastic dynamics and the modern, obliquity-dominated, orbital theory.

2 The orbital theory

We use the term 'orbital theory', originally proposed by Bolshakov (2008), to describe the hypothesis that global climate is affected by changes in Earth's orbital characteristics, such as the *eccentricity*, the *precession* of the equinoxes and the axial tilt or *obliquity*, at scales ranging from 20 to 100 thousand years or even more (Berger, 1978). This hypothesis was set forth by Milankovitch (1941), following the theoretical ideas of Adhemar (1842; from Imbrie 1982) and Croll (1864; from Imbrie 1982). According to it, the intensity of incoming solar radiation during the summer solstice at high latitudes (65^{o}) of the northern hemisphere (Figure 1a) causes the glaciation and deglaciation periods. Direct insolation changes by eccentricity or insolation at the southern hemisphere are not regarded to have a clear effect to climate as underlined by several researchers (Imbrie et al. 1993; Liu and Chao 1998; Balshakov 2008; Huybers 2009), despite the fact that it has been shown that the glaciations were almost synchronous in both hemispheres (Kawamura et al. 2007). Rather, glaciation cycles are mainly affected by precession forcing (19 and 24 thousand years) and obliquity forcing (41 thousand years). Thorough reviews of the historical development of the theory, as well as a full description of the celestial mechanics, are presented by Imbrie (1982), Bolshakov (2008) and Paillard (2010).

Recently, the orbital climate theory has been challenged by several studies arguing that it cannot sufficiently describe the links between climate and insolation variations (Winograd et al. 1992; Muller and MacDonald 2000; Elkibbi and Rial 2001; Wunsch 2004; Bolshakov 2008). A well-known example of the weaknesses of the orbital theory is the mid-Pleistocene transition (MPT), which refers to the switch, around 900 thousand years BP, from predominant 41 thousand years glaciation cycles to 100 thousand years glaciation cycles. This transition occurred without a corresponding change in orbital forcing (Pisias and Moore 1981) and the duration of each of the last four glacial cycles increased from 80 to 130 thousand years, which suggests that major climate shifts were aperiodic (Winograd et al. 1992). Till today, there is no confirmed explanation for MPT, although some efforts have been made and some hypotheses have been formulated, including those of a glacial-modulated threshold (Paillard 1998), frequency modulation (Rial 1999), possible CO_2 correlation (Berger et al. 1999) and obliquity-modulated threshold (Huybers 2006).

An alternative path to the understanding of the global climate cycles was based on stochastic dynamics (Petersen and Larsen 1978; Kominz and Pisias 1979; Benzi et al. 1982; Saltzman 1982; Pelletier 2003; Ditlevsen 2009). In this concept, insolation forcing could have a minor role in the glaciation cycles, or even could have no role at all, whereas the self-sustained internal variability of the climate system could be the actual driver of the glaciations (Ashkenazy and Tziperman 2004). Small periodic perturbations could be amplified by the variability of the climate system through the mechanism of stochastic resonance (Benzi et al. 1982), which was based on the works of Hasselmann (1976) and Sutera (1981). The former demonstrated that short-time-scale phenomena, modelled as stochastic perturbations, could affect long-term climate variations. The latter showed that if such stochastic perturbations are imported into an energy balance model with no other forcing, they could lead to random transitions between the equilibrium states of the model.

In the last few years, there has been an effort to bridge the gap between the classical orbital theory and stochastic dynamics. Huybers and Wunsch (2005) proposed that obliquity may be a more important mechanism of glacial dynamics, in a nonlinear way though, and showed that the integrated summer insolation at high latitudes is relevant to the obliquity cycle (Figure 1b). Their suggestion was supported recently by high resolution empirical data (Liu et al. 2007; Suwa and Bender 2008; Drysdale et al. 2009; Naish et al. 2009; Lourens et al. 2010) and as Paillard (2010) highlights: "*the relative weight of 23 000 and 41 000 years periodicities is quite different with such a definition of the astronomical forcing, pleading for a more prominent role of obliquity on climate than usually assumed*". An important addition to the development of *modern orbital theory* is the mechanism of nonlinear phase locking, describing a mechanism in which obliquity can act as a pace maker for the glacial periods, amplified by the internal system dynamics (Gildor and Tziperman 2000; Ashkenazy 2006; Tziperman et al. 2006). On the other hand, Roe (2006) showed that insolation is in good agreement with the change in ice volume (dV/dt) for the last million years, which led to further investigation of possible combination of obliquity and precession forcing (Huybers and Tziperman 2008, Huybers 2011).

A simple comparison (Figure 2) between the spectra of Milankovitch' insolation (Laskar et al. 2004), integrated insolation (Huybers 2006) and a temperature reconstruction (Huybers 2007) indicates some resemblance between the spectra of integrated insolation and temperature in terms of merely the

obliquity cycle. Namely, they all share a peak at the periodicity of 41 thousand years, but the last one has also one at 100 thousand years. To see whether peaks in the spectrum of the latter series represent regular periodicities or are the result of random effects, we can divide the time series whose spectrum is presented in Figure 2c in two or three equal parts and then compare the power spectra of the different parts: If a peak spotted in the spectrum represents a true deterministic periodicity, then it should be found in the spectra of all parts, while peaks that are due to random perturbations or random sampling would not appear in some of the parts. (We could continue this technique by splitting to four parts, etc., but this would reduce the sub-sample size and the reliability of statistical estimates too much).

In this case, the only signal that remains detectable in almost all spectral densities is the one from obliquity (Figures 3 and 4, respectively). Even in the obliquity signal, in one of the sub-samples corresponding to the earliest period of the proxy record, the 41 thousand years periodicity disappears (the amplitude vanishes off) or shifts to lower values (around 38 thousand years; Figure 4). Through this simple analysis we can verify that the 41-thousand-year signal is most likely to represent a real periodicity, which is also supported by other widely used reconstructions of this period, like that of Lisiecki and Raymo (2005) and findings using wavelet analysis (Liu and Chao, 1998).

In conclusion, the debate about the exact physical mechanisms which influence the emergence of glaciation and deglaciation is still ongoing. This extends to a wider discussion about the overall deterministic or stochastic character of the glacial periods and the possible links between them. In this dissent, one has to notice that determinism and uncertainty should not necessarily be regarded as two opposite notions (Koutsoyiannis 2010), but rather as the two sides of the same coin. Here the metaphor of a coin with its two sides may prompt us to think that its trajectory when flipped, although far too simpler than climate evolution, ironically, has an outcome that nobody is keen to describe deterministically.

3 The omnipresence of the HK behaviour

In contrast to the orbital theory, which suggests a link between a few characteristic periodicities in insolation and the climate system, the HK behaviour is related to irregular fluctuations on all time scales. Since its original discovery by Hurst, the HK behaviour has been identified in several hydrological studies regarding the flows of several rivers such as the Nile (Hurst 1951; Eltahir 1996;

Koutsoyiannis 2002), Warta, Poland (Radziejewski and Kundzewicz 1997), Boeoticos Kephisos, Greece (Koutsoyiannis 2003a), Nemunas, Lithuania (Sakalauskienė 2003) and Yangtze, China (Jiang et al. 2005; Wang et al. 2006); low flows in 250 hydrometric stations in Canada (Ehsanzadeh amd Adamowski 2010); monthly runoff data in Malaysia (Ramachandra Rao et al. 2011); the inflows of Lake Maggiore, Italy (Montanari et al. 1997); and droughts in Europe (Bordi et al. 2009) and North America (Padmanabhan et al. 2008).

In addition, the HK behaviour has gained new interest today due to its relation to climate changes (e.g. Evans, 1996; Koutsoyiannis, 2003a, b). Indeed, the HK behaviour has been identified in many climatic or meteorological quantities such as in wind power (Haslett and Raftery 1989, Bouette et al. 2006, Bakker and Hurk 2011); atmospheric or oceanic processes and temperature in particular (Bloomfield 1992; Koscielny-Bunde et al. 1998; Koutsoyiannis 2003a,b, Fraedrich and Blender 2003, Yano et al. 2004, Varotsos and Kirk-Davidoff 2006, Alvarez-Ramirez et al. 2008, Fraedrich et al. 2009); regional and global convective precipitation (Riemann-Campe et al. 2011) and regional precipitation measured by radars (Maurizio et al. 2011); and indices of North Atlantic Oscillation (Stephenson et al. 2000) and Pacific Decadal Oscillation (Khaliq and Gachon 2010). Bunde et al. (2005) found that the scaling behaviour leads to pronounced clustering of extreme events and demonstrated that this can be seen in long climate records, while Lennartz and Bunde (2011) examined how this affects the recent trends in global temperature, precipitation and runoff.

HK dynamics is not restricted only to hydro-meteorological processes, but it is present in other natural processes, including geological phenomena like seismicity (Teleska et al. 2000, Mukhopadhyay et al. 2008). It is also found in phenomena of biological character such as the patterns of DNA sequences (Peng et al. 1994, Stanley et al. 1996); the molecular motion in cell membranes (Sheng et al. 2011); medical indices for heart failure (Lin et al. 2001, Beckers et al. 2006); brain aging (Bernard et al. 2006); and immature preterm infants breathing patterns (Navarro et al. 2011). The latest findings in the field of neurobiology concerning the functional Magnetic Resonance Imaging technique, suggest that the Hurst coefficient (see definition below) can be used as a biomarker for certain disorders including Alzheimer (Maxim et al. 2005), Parkinson (Rassouli 2006), autism (Lai 2010) and impulsive traits (Hahn et al. 2012). Finally, it is remarkable that scaling behaviour has been also identified in certain artificial processes, such as network traffic (Leeland 1994, Karagiannis et al. 2004) or econometrics (Lo 1991, Baille 1996, Serinaldi 2010). For instance, in the field of economy, the scaling

behaviour has been detected in energy prices (Serletis and Rosenberg 2007), financial markets (Gama et al. 2008) and Spanish electricity spot market (Norouzzadeh et al. 2007).

In the field of paleoclimatology, several studies have examined the long term statistical properties of proxy data and their possible consistency with the HK dynamics. Shackleton and Imbrie (1990) were the first to investigate spectral properties of eight of the first available climatic proxy datasets, over a range of 340 thousand to 130 million years. Their spectra appeared to have negative slopes, which is typical in HK dynamics (Beran 1994); however, their sample sizes where small (~440 on average). Their findings were supported by Pelletier (1997), who divided the power spectrum of atmospheric temperatures in four regions of power-law behaviour for the last million years. Moreover Richards (1994), detected an HK behaviour for the ice core proxy data from Greenland (GRIP data set; see below), which was also confirmed by more recent findings for another data set from Greenland (GISP2 data; Koutsoyiannis et al. 2009; see also below). Similar results were obtained from other ice core data from Antarctica and Greenland at time scales of 1-100 thousand years (Ashkenazy et al. 2003). Furthermore, Koutsoyiannis (2002) detected HK behaviour in tree-ring proxies, while Rybski et al. (2006) followed by Koutsoyiannis and Montanari (2007) examined six multi-proxy time series, spanning from 580 to about 2000 years, all of which were found to exhibit HK behaviour.

A possible explanation for the presence of HK dynamics in so many different processes can be found by examining the related statistical behaviour. Koutsoyiannis (2002) proposed that HK dynamics could be the outcome of fluctuations of the process at a multitude of time scales; an idea also found in the work of Klemes (1974) and Mesa and Poveda (1993). Namely, Koutsoyiannis (2002) demonstrated that if we add three Markov (AR(1)) processes with different autocorrelation coefficients (representing three time scales), then their sum approximates a HK process. Moreover, Koutsoyiannis (2011a) has shown that application of the principle of the maximum entropy production in a stochastic framework can result in HK dynamics.

In this study we provide a more extensive investigation of the possible presence of HK dynamics in paleoclimatic series and instrumental data sets. In particular, the proxy records we examine cover a much larger period going back up to ~500 million years as described below.

4 Data used

Since instrumental data are available only for a very short period of the recent past (Broehan et al. 2006), new methods have been developed in the last 35 years to explore climatic variability at larger scales. Paleoclimatic reconstructions of local or global climatic variables use proxy data such as the $^{18}O/^{16}O$ isotope ratio (or its relative difference, $\delta^{18}O$, from a standard, such as the Vienna Standard Mean Ocean Water), pollen records, tree rings and many other, to infer the values of climatic variables, i.e. temperature, humidity, etc. Each of these proxy time series types has different time length, temporal coverage and time resolution, depicting only a part of the total climatic variability. For a more general overview, in our study we use ten temperature-related time series with time steps spanning from monthly to 500 thousand years and overall lengths from 30 years to ~500 million years, as summarized in Table 1 (labelled by the name of first author or project).

The highest resolution time series used are instrumental, based on satellite (NSSTC) and ground (CRU) data (Figure 5a). The satellite record is characterized by global spatial coverage, while CRU data represent a fivefold time length (161 years against 32 of NSSTC). To reduce the effect of seasonality (within-year variability), both time series whose time step is monthly are temperature deviations from monthly averages (of the reference period 1961-1990). The temperature deviations measured by satellites have a rising trend of 1.37°C/century whereas station data for the same period indicate a somewhat larger trend.

We can move to a coarser scale with the help of the annual-scale, multi-proxy, global temperature reconstructions of Moberg (2005) and Lohle (2007) (Figure 5b), where the former is based on tree-rings, boreholes, cave stalagmites and sediment data, while the latter adds pollen data but leaves out tree ring data. In these series, in addition to the recent warming trend, we observe that rising or falling trends are also present in other periods. For example, in the Moberg reconstruction at a 30–year time window we can locate a 1.7°C/century rise before the Medieval Warm Period (MWP) or a 2.2°C/century decrease before the Little Ice Age (LIA) in the 16th century. These become milder in the Lohle reconstruction, which is expected because that series is smoothed at the 30-year scale.

Ice cores give us information for the last 800 000 years (Figure 6) by the use of the isotope deuterium (δD) or the isotope ratio $\delta^{18}O/\delta^{16}O$, which is assumed to be linearly proportional to temperature (Dansgaard et al. 1993; Steig et al. 1999; Jouzel et al. 2007). We have used proxy data

extracted from three one-site ice cores: Taylor Dome in Antarctica for the 10 000 years of the undergoing interglacial period (Figure 6a), GRIP in Greenland for the last 100 000 years (Figure 6b) and EPICA, also in Antarctica, for the last 9 glaciations/deglaciations (Figure 6c). The ice-core and sediment reconstructions had varying time step and were converted by linear interpolation to constant time step, close to the largest value of the varying raw time step. The interpolation does not alter the results as will be demonstrated below. To maintain a satisfactory sample size, in the cases of Taylor and GRIP reconstructions, we used only the highest resolution fraction of each time series (note that the time step increases at the earliest times of the series; see Table 1).

Finally, to see farther in the past, we use global reconstructions from multi-site ocean sediment depositions, based also on the $\delta^{18}O/\delta^{16}O$ ratio (Figure 7). The oscillating pattern of glaciers' extension and retreat, already seen in EPICA and GRIP data (Figures 6b and 6c), becomes even more evident in the Huybers time series in the last 2.5 million years (Figure 7a). A 0.2°C/million years decreasing trend in global temperature has been prevailing in the last 50 million years (Figure 7b), while the most important events in the last 500 million years are the icehouse periods described above, which are seen in the Veizer time series as low-temperature periods (Figure 7c). This decreasing trend and the icehouse periods demonstrate that time scales of fluctuation, represented by HK dynamics, can be very large.

5 Methods of analysis

5.1 Multiscale representation of stochastic processes

By its definition, climate involves averaging of a continuous time process $\underline{x}(t)$, such as air temperature, at various time scales k (notice the notational convenience, known as the Dutch convention, to underline random variables and stochastic processes; here $\underline{x}(t)$ is assumed to be a scalar quantity).

The transformation of the instantaneous-time process $\underline{x}(t)$ into a discrete time process $\underline{x}_i^{(k)}$ at time i and scale k, is given as

$$\underline{x}_i^{(k)} := \frac{1}{k} \int_{(i-1)k}^{ik} \underline{x}(t)dt \qquad (1)$$

and is referred to as the averaged process at time scale k. While the instantaneous process $\underline{x}(t)$

represents the "weather", for sufficiently large k (e.g., $k > 30$ years), $\underline{x}_i^{(k)}$ represents the climate.

The climatic variability is naturally quantified by the standard deviation $\sigma^{(k)}$ of $\underline{x}_i^{(k)}$. A key tool that provides a multi-scale stochastic characterization is the plot (typically double logarithmic) of $\sigma^{(k)}$ versus k, which has been termed the climacogram (from the Greek climax, i.e., scale; Koutsoyiannis, 2010—not to be confused with the climatogram). The climacogram resembles the fluctuation function used in the detrended fluctuation analysis (DFA), and, in particular, the so-denoted DFA0 method, in which no trend filtering is used (Eichner et al., 2003). Yet the two notions have some differences. Namely, the climacogram uses just one single notion, the standard deviation, with its exact meaning in probability and statistics. Consequently, the standard deviation $\sigma^{(k)}$, as a function of k, can be calculated for a certain theoretical model using probability theory and in this case we call it the "theoretical climacogram". It can also be estimated by statistical calculations (i.e. from the standard estimator of standard deviation) using data (time series) and in this case we call it the "empirical climacogram".

The climacogram is simpler and more robust than other commonly used stochastic tools, i.e., the power spectrum (already used in several studies as discussed above) and the autocorrelogram, and it is related to them by simple transformations (Koutsoyiannis 2010). In addition, as will be seen below, the climacogram is powerful, offering easy means to combine views of different time series in a single graph (Figure 9 to be discussed later).

A fully deterministic, strictly periodic process composed of a single harmonic with period T has a climacogram of the form (see Appendix A)

$$\sigma^{(k)} = |\mathrm{sinc}(k/T)| = [T/(\pi k)]\,|\sin(\pi k/T)| \tag{2}$$

where sinc denotes the normalized sine-counting function. However, in a process affected by many cycles with different periods T, the climacogram, obtained by considerations of extremal entropy production (Koutsoyiannis 2011a), is given by the simple power-law relationship

$$\sigma^{(k)} = k^{H-1}\,\sigma \tag{3}$$

where $\sigma \equiv \sigma^{(1)}$ and H is the entropy production in logarithmic time, more commonly known as the Hurst coefficient and takes on values between 0 and 1. Thus, (3) represents a natural behaviour (the HK behaviour, described in section 3), defines a stochastic process exhibiting this behaviour (the HK process), and describes the stochastic dynamics of this process (the HK dynamics).

In Figure 8, some typical mathematical processes are illustrated in terms of their

climacograms, starting with the common white noise process, which is characterized by independence in time. This purely random process is a specific case of the HK process, in which $H = 0.5$, so that $\sigma^{(k)} = \sigma/k^{0.5}$, which implies a constant slope $\theta = -0.5$ in the climacogram (where generally the slope is defined as $\theta := \mathrm{d}(\ln \sigma^{(k)}) / \mathrm{d}(\ln k)$). On the other hand, in the deterministic, periodic process of equation (2) with period T (=100 in Figure 8) the climacogram has an oscillating shape with an upper envelope with a steep slope $\theta = -1$, but the local slope can be even steeper, tending to $\pm\infty$ at values of k that are integer multiples of T (see proof in Appendix A and illustration in Figure 8).Another common stochastic process is the simple Markov process or, in discrete time i, the autoregressive process of order 1 (AR(1)), which exhibits dependence expressed at scale 1 as

$$\underline{x}_i = \rho\, \underline{x}_{i-1} + \underline{v}_i \tag{4}$$

where ρ stands for the lag-one autocorrelation coefficient ($-1 < \rho < 1$) and $\underline{v}_i$ (i = 1, 2, …) are independent, identically distributed, random variables. In this case the climacogram is given by the equation (Koutsoyiannis 2002)

$$\sigma^{(k)} = \frac{\sigma}{\sqrt{k}} \sqrt{\frac{(1-\rho^2) - 2\rho(1-\rho^k)/k}{(1-\rho)^2}} \tag{5}$$

which in the example plotted in Figure 8 (for $\rho = 0.75$) decays to a slope equal to that of a purely random process ($\theta = -0.5$, Koutsoyiannis 2002) for scales larger than ~10. In contrast, the climacogram of the HK process maintains a constant slope $\theta = H - 1$, as inferred from equation (3). When $H > 0.5$, this slope becomes milder ($\theta > -0.5$) than in a purely random process and indicates long-term persistence, as contrasted to the short-term persistence represented by the AR(1) model. This is illustrated in the example of Figure 8, in which $H = 0.9$, so that the lag-one autocorrelation coefficient is roughely the same as in the AR(1) model, i.e. $\rho = 0.75$. For small scales the climacograms of the AR(1) and HK models are almost identical but for large time scales they markedly diverge. HK processes with H in the range 0.5 to 1 result in climacogram slopes θ between –0.5 and 0 and are called persistent (whereas HK processes with $H < 0.5$ are called anti-persistent). For large (climatic) scales k these are less predictable than white noise or Markov processes, in which $\theta = -0.5$, because their standard deviation of the averaged process is reduced by a smaller rate as scale k increases. This indicates that the variation of standard deviation with scale becomes important in characterizing predictability, particularly at large (climatic) scales.

5.2 Construction of the combined climacogram

Theoretical climacograms, like those of Figure 8, are readily constructed as the theoretical standard deviation of any specific stochastic process at any scale is easy to calculate. Likewise, a specific time series can give an empirical climacogram based on the classical sample estimates of the standard deviation $\sigma^{(k)}$ for several aggregate scales k.

Thus, each of the ten data series allows the construction of an empirical climacogram for aggregate scales k spanning from the available resolution Δ (shown in Table 1) up to $k = L/10$ (with L being the total length of the time series shown in Table 1). With the latter choice the sample of the averaged process $\underline{x}^{(k)}$ has at least 10 data points for the estimation of $\sigma^{(k)}$, as proposed by Koutsoyiannis (2002). Thus, to construct the empirical climacogram we calculate an averaged time series for each scale (k = 1, 2, 3, ..., $L/10$) and then calculate the sample estimate of the standard deviation $\sigma^{(k)}$. In order to confirm that linear interpolation on the data does not introduce an error on the climacogram, we compared it with the closest-point estimation (see Appendix B).

Once we have calculated the climacograms of all ten time series, we can superimpose them to construct a combined climacogram representative for time scales ranging from monthly to 50 million years (i.e., one tenth of the length of Veizer series which is ~500 million years). Since the units of the various series differ, those of standard deviations will differ too. For this reason, the climacograms of the different series are not fully compatible to each other, but appropriate linear transformations thereof should be compatible as they all reflect temperature.

Here we are interested in the variation of standard deviation with scale, rather than the precise values of standard deviation. Thus, we can impose normalization by multiplying each climacogram by a constant value, determined so as to match the different climacograms. Assuming that a time series $y(t)$ is a proxy of a process $x(t)$ and the two are, as an approximation, connected by a linear relationship $x(t) = a\, y(t) + b$, the two climacograms $\sigma_x^{(k)}$ and $\sigma_y^{(k)}$ will be related as $\sigma_x^{(k)} = a\, \sigma_y^{(k)}$. For the first time series (NSSTC) we arbitrarily selected a_1 so that $\sigma_1^{(k)} = 1$ for k = 1/12 year (1 month). For the other nine series we calculated a unique set of weights a_2, ..., a_{10}, by minimizing the departures among the $\sigma^{(k)}$ of the different series for the same scale k. Specifically, we have chosen characteristic time scales $k_l = 2^l$ years with l varying from –3 to 22 (k_l varying from 0.125 to 4194304 years) and we interpolated each climacogram at those points k_l that fall into the domain of the empirical climacogram (as depicted in Figure 9). For each k_l we formed a sample of empirical climacogram values obtained by each of the

different series that were overlapping at a range containing the point k_l. We then estimated the sample standard deviations at all points k_l and we minimized their sum for all k_l. For the (unconstrained) minimization we used the Generalized Reduced Gradient method (Lasdon et al., 1978; Lasdon and Smith, 1992) which is one of the most robust and reliable approaches to nonlinear optimization and has become commercially available as an easy Solver tool embedded in EXCEL. By direct application of this Solver we obtained a unique set of the ten weights a_1, ..., a_{10} that minimizes the above sample of standard deviations. With this set of weights we made the logarithmic plot shown in Figure 9.

6 Discussion

The combined climacogram of Figure 9 gives us an impressive overview of climatic variability spanning almost 9 orders of magnitude—from 1 month to 50 million years. We observe that, for this huge variation of the scale k, the $\sigma^{(k)}$ of all series range in a small interval, varying less than an order of magnitude (between 0.1 and 1). This can be contrasted to a purely random climate, which would entail a climacogram quickly descending (with slope –0.5, also depicted in Figure 9) to lower orders of magnitude. Overall, the combined climacogram indicates a very mild slope of about –0.08, suggesting a strong HK behaviour. A slope of –0.08 in a theoretical climacogram would correspond to $H = 0.92$, but here the climacogram is empirical and thus possibly negatively biased (Koutsoyiannis 2003). Thus, we can regard the value 0.92 as a lower bound of H and this suffices for the purpose of the paper which is to demonstrate the presence of HK behaviour rather than to propose an exact model. However, even this lower bound is a very high value, yet compatible with previous results (e.g. Koutsoyiannis and Montanari 2007) and implies spectacular differences from the classical statistics (in which the consecutive values are independent), as well as from typical stochastic processes like the Markov process. Classical statistics has served as the common basis of interpreting climate behaviours, and performing statistical tasks such as estimation and hypothesis testing.

The horizontal line in Figure 9 (drawn from the rightmost point of the straight line fitted to the empirical climacogram, which has slope -0.08) shows that the climatic variability at the scale of 100 million years is about 19% of the variability at the monthly scale. If climate was consistent with classical statistics, the reduction of variability to 19% (from 100% in the monthly scale) would appear at the scale of 28 months (the intersection of the horizontal line with the line with slope –0.5). This dramatic difference (28 months vs. 100 million years), suggests enhanced change particularly at large

time scales and, hence, enhanced unpredictability, as climatic variability remains high even for the largest time scales. This should help us understand that the classical statistical thinking may be inappropriate for climate and that the classical dichotomy of weather versus climate may be misleading.

Several "imperfections" can be observed in the matching of the climacograms of the different time series in Figure 9. These are not unexpected, and they themselves are the result of data uncertainties (both in sampling and aging) combined with the bias and enhanced uncertainty, which are implied by the long-term persistence in statistical estimation (Koutsoyiannis 2003, 2011b). In some cases, the right part of a climacogram is too flat, as for example in Zachos and CRU time series. The reason for a flat right part is related to the fact that the entire time series length is located on a branch of the process with a monotonic trend (Figure 7). When a longer time series is viewed (Veizer for Zachos, Moberg and Lohle for CRU), which shows that the monotonic trend is in fact part of a longer fluctuation, the flat climacogram problem is remedied.

One of the most prominent "imperfections" of Figure 9 is related to the Huybers and EPICA climacograms, both of which have leftmost and rightmost parts with slopes milder and steeper, respectively, than the general slope. Particularly in the EPICA case, the rightmost part has a slope steeper than –0.5, which could be interpreted as indicating anti-persistence. However, this behaviour can be attributed to the combined effect of statistical bias and the influence of the orbital forcing. To demonstrate that the "imperfection" is in fact the result of the Milankovitch cycles acting at time scales in the range of 10^4 – 10^5 years, we have constructed an explanatory toy model, from which we constructed the climacograms of Figure 10. This toy model represents the synthesis of the theoretical climacograms of three components. Namely, we consider the sum of an HK process with $H = 0.92$ and two harmonics with periods 100 and 41 thousand years with weights shown in the figure caption. We note that this toy model is not unique; several other could be constructed by also including a 21 thousand years harmonic and by changing the weighs of the three or four components. We selected to present the one in Figure 10 (as an explanatory tool and not as a model to be used in applications), because it is the most parsimonious among those examined and corresponds to the dominant role obliquity in modern orbital theory.

The theoretical climacogram of the toy model (whose mathematical expression is simply $\underline{x}(t) = a_H\underline{x}_H(t) + a_1x_1(t) + a_2x_2(t)$, where $\underline{x}_H(t)$ is an HK process, $x_1(t)$ and $x_2(t)$ are harmonics with periods 100

and 41 thousand years, respectively, and the values of the coefficients a_H, a_1, a_2 are given in the caption of Figure 10) can be readily calculated from (2) and (3). As a result of the two harmonics, the slope of the theoretical climacogram at scales approaching 10^5 years is much steeper than –0.08, showing a similar shape to the real-world climacogram. In addition, using the toy model we can generate a series with resolution and length equal to those of the EPICA series, in order to explore the statistical effects and particularly the negative bias. The resulting empirical climacogram of one synthetic time series, also plotted in Figure 10, resembles the real EPICA climacogram of Figure 9.

Generally, the steeper slope at time scales between 10 and 100 thousand years suggests higher predictability over those scales in comparison to shorter or longer scales, but again this does not counteract the enhanced uncertainty and unpredictability entailed by the overall HK dynamics. This uncertainty is magnified by the fact that, as already mentioned, the orbital forcing cycles are not apparent all the time and are not strictly periodic (see also Richards 1994; Ashkenazy et al. 2003).

Interestingly, similar behaviours, represented by a climacogram with a similar shape can be found in other natural processes as well, such as the sunspot number (Figure 11). In this case, the steeper slope emerges at scales between 5 and 13 years (55 and 143 months), reflecting the connection between the 11 year sunspot 'cycle' and the stochastic behaviour of the phenomenon in the same manner exhibited by the toy model in Figure 10.

7 Conclusions

The available instrumental data of the last 160 years allow us to see that there occurred climatic fluctuations with a prevailing warming trend in the most recent past. However, when this period is examined in the light of the evidence provided by paleoclimate reconstructions, it appears to be a part of more systematic fluctuations; specifically, it is a warming period after the 200-year 'Little Ice Age' cold period, during a 12 000-year interglacial, which is located in the third major icehouse period of the Phanerozoic Eon. The variability implied by these multi-scale fluctuations, typical for Earth's climate, can be investigated by combining the empirical climacograms of different paleoclimatic reconstructions of temperature. By superimposing the different climacograms we obtain an impressive overview of the variability for time scales spanning almost 9 orders of magnitude—from 1 month to 50 million years.

Two prominent features of this overview are (a) an overall climacogram slope of –0.08,

supporting the presence of HK dynamics with Hurst coefficient of at least 0.92, and (b) strong evidence of the presence of orbital forcing (Milankovitch cycles) at time scales between 10 and 100 thousand years. While orbital forcing favours predictability at the scales it acts, the overview of climate variability at all scales clearly suggests a big picture of enhanced change and enhanced unpredictability of Earth's climate, which could be also the cause of our difficulties to formulate a purely deterministic, solid orbital theory (either obliquity or precession dominated). Endeavours to describe the climatic variability in deterministic terms are equally misleading as those to describe it using classical statistics. Connecting deterministic controls, such as the Milankovitch cycles, with the Hurst-Kolmogorov stochastic dynamics seems to provide a promising path for understanding and modelling climate.

Acknowledgements We thank Prof. Zbigniew W. Kundzewicz for his encouraging and detailed comments on an earlier short version of this manuscript. We also thank the Editor Dr. Michael Rycroft for his encouragement to create this expanded version of the paper, an anonymous reviewer for his positive reception of our work, and the eponymous reviewer Dr. B. De Saedeleer for his detailed and constructive review.

Appendix A. Proof of equation (2)

We assume a fully deterministic, strictly periodic process composed of a single harmonic with period T, described by,

$$x(t) = \sqrt{2}\ \cos(2\,\pi\,t\,/\,T + b) \qquad \text{(A1)}$$

It can be seen that during the time interval $[t_1, t_2]$, where $2\,\pi\,t_{1,2}\,/\,T + b = \pm\arccos(x/\sqrt{2}\,)$, the process $\underline{x}(t)$ takes on values greater than or equal to x, provided that $-\sqrt{2}\ \le x \le \sqrt{2}$ (see Fig. A1). The length of the interval $[t_1, t_2]$ is $(T/\pi)\arccos(x/\sqrt{2}\,)$. Consequently, if we treat the process $x(t)$ stochastically, it follows that its marginal distribution function is

$$F(x) = 1 - \arccos(x/\sqrt{2}\,)/\pi,\ -\sqrt{2}\ \le x \le \sqrt{2} \qquad \text{(A2)}$$

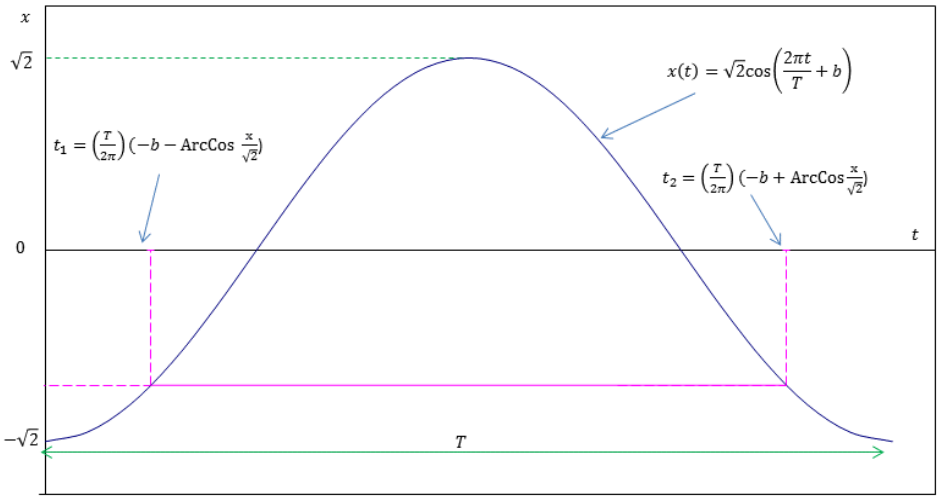

Figure A1 Sketch to illustrate the proof of (A2). For the ease of the illustration it was assumed $b = \pi$, but this does not affect the result neither the length of the time interval, which does not depend on b.

Taking its derivative with respect to x, we find its marginal density function as

$$f(x) = 1/(\pi\sqrt{2 - x^2}\,),\ -\sqrt{2}\ \le x \le \sqrt{2} \qquad \text{(A3)}$$

By application of definitions of mean and variance, we readily obtain that the mean of the process is 0,

and its variance is 1. Likewise, the process autocovariance is:

$$R(\tau) = \mathrm{cov}[\underline{x}(t), \underline{x}(t+\tau)] = E[\underline{x}(t)\,\underline{x}(t+\tau)] \tag{A4}$$

where τ is lag time. If $x(t) = x$ then $t = (T / 2\pi)\,[-b + \arccos(x/\sqrt{2}\,)]$ (one of the infinitely many possibilities), so that $t + \tau = (T / 2\pi)\,[-b + \arccos(x/\sqrt{2}\,)] + \tau$ and $x(t+\tau) = \sqrt{2}\,\cos[2\,\pi\,\tau / T + \arccos(x/\sqrt{2}\,)]$. Consequently,

$$R(\tau) = \sqrt{2}\int_{-\sqrt{2}}^{\sqrt{2}} x\cos[2\pi\tau/T + \arccos(x/\sqrt{2}\,)]\,f(x)\,\mathrm{d}x \tag{A5}$$

which after algebraic manipulations becomes

$$R(\tau) = \cos(2\,\pi\,\tau / T) \tag{A6}$$

Interestingly, this does not depend on t, thus behaving like a stationary process.

The climacogram value at scale k can be calculated from the variance $\mathrm{Var}[\,\underline{x}_i^{(k)}\,]$, i.e.,

$$\mathrm{Var}[\,\underline{x}_i^{(k)}\,] = E[\{\,\underline{x}_i^{(k)}\,\}^2] = \frac{1}{k^2}\int_0^k\int_0^k E[x(t)\,x(s)]\,\mathrm{d}t\,\mathrm{d}s \tag{A7}$$

or

$$\mathrm{Var}[\,\underline{x}_i^{(k)}\,] = \frac{1}{k^2}\int_0^k\int_0^k R(t-s)\,\mathrm{d}t\,\mathrm{d}s = \frac{1}{k^2}\int_0^k\int_0^k \cos[2\,\pi\,(t-s)/T]\,\mathrm{d}t\,\mathrm{d}s \tag{A8}$$

which after algebraic manipulations becomes

$$\mathrm{Var}[\,\underline{x}_i^{(k)}\,] = [T/(\pi\,k)]^2\sin^2(\pi\,k/T) \tag{A9}$$

By taking the square root of $\mathrm{Var}[\,\underline{x}_i^{(k)}\,]$, which by definition is the standard deviation $\sigma^{(k)}$, this gives equation (2).

From (2) we readily infer that for increasing k there appears a series of maxima at values $k = \alpha T/2$, with α any odd integer, so that $|\sin(\pi\,k/T)| = 1$. This series is described by $\sigma^{(k)} = T/(\pi\,k)$, which is an upper envelope curve of the climacogram. Obviously, across this envelope, $\theta = \mathrm{d}(\ln\sigma^{(k)}) / \mathrm{d}(\ln k) = -1$. However, the local slope of the climacogram is not constant but varies. We can easily determine it from

$$\theta := \mathrm{d}(\ln \sigma^{(k)}) / \mathrm{d}(\ln k)) = (k/2)\, \mathrm{d}\{\ln [\sigma^{(k)})^2]\} / \mathrm{d}k = (k/2)\, \mathrm{d}(\ln \{[T/(\pi k)]^2 \sin^2(\pi k/T)\} / \mathrm{d}k \quad \text{(A10)}$$

which after algebraic manipulations becomes

$$\underline{\theta} = (\pi k/T) \cot(\pi k/T) - 1 \quad \text{(A11)}$$

It can be seen that θ tends to $\pm \infty$ whenever k/T is integer.

Appendix B. Assessment of the interpolation effect on the climacogram

In order to examine possible effects of the linear interpolation to the data we compared it with the closest-point estimation. In the latter, we estimate the unknown value at a specific time using the value of the given time series at the point closest to this specific time (without doing any calculation). As shown in Figure B1, where the climacograms estimated by both interpolation methods for the GRIP time series are depicted, the results of the two methods are virtually indistinguishable, which means that in the case examined the climacogram is practically indifferent to the type of interpolation.

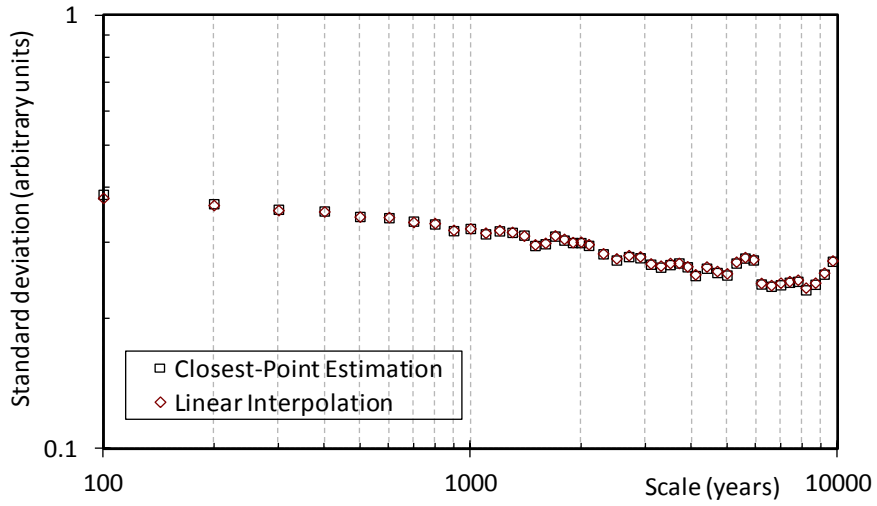

Fig. B1 Climacogram for the GRIP data set calculated from the time series constructed by linear interpolation in comparison to that of the time series constructed by closest-point estimation.

References

Adhemar J A (1842) Revolutions de lamer. Privately published, Paris

Agassiz L (1840) Etudes sur les glaciers. Privately published, Neuchatel

Alley RB, Meese DA, Shuman CA, et al. (1993) Abrupt increase in Greenland snow accumulation and the end of the Younger Dryas event. Nature 362:527–529

Alvarez-Ramirez J, Alvarez J, Dagdug L, Rodriguez E, Carlos Echeverria J (2008) Long-term memory dynamics of continental and oceanic monthly temperatures in the recent 125 years. Phys A 387(14):3629-3640

Ashkenazy Y, Baker DR, Gildor H, Havlin S (2003) Nonlinearity and multifractality of climate change in the past 420 000 years. Geophys Res Lett. doi:10.1029/2003GL018099

Ashkenazy Y, Tziperman E (2004) Are the 41 kyr glacial oscillations a linear response to Milankovitch forcing? Quat Sci Rev 23(18-19):1879-1890

Ashkenazy Y (2006) The role of phase locking in a simple model for glacial dynamics. Clim Dyn 27(4):421-431

Baillie RT (1996) Long memory processes and fractional integration in econometrics. J Econometrics 73:5–59

Bakker AMR, Hurk BJJM (2011) Estimation of persistence and trends in geostrophic wind speed for the assessment of wind energy yields in Northwest Europe. Clim Dyn. doi: 10.1007/s00382-011-1248-1

Beckers F, Verheyden B, Couckuyt K, Aubert AE (2006) Fractal dimension in health and heart failure. Biomed Eng 51(4):194-197

Benzi R, Parisi G, Sutera A, Vulpiani A (1981) Stochastic resonance in climatic change. Tellus 34 (1):10–6

Beran J (1994) Statistics for long-memory processes, Chapman & Hall, New York

Berger AL (1978) Long- term variations of daily insolation and Quaternary climatic changes. J Atmos Sci 35:23622367

Berger A, Li XS, Loutre MF (1999) Modelling northern hemisphere ice volume over the last 3 Ma. Quat Sci Rev 18:1–11

Bernard F, Salvador R, Bullmore E, Suckling J, Wink AM (2006) Age and cholinergic effects on

hemodynamics and functional coherence of human hippocampus. Neurobiol Aging 27(10):1395-1404

Bloomfield P (1992) Trends in global temperature. Clim Change 21:1-16

Bolshakov VA (2008) How long will the 'precession epoch' last in terms of Pleistocene glacial cycles? Rus J Earth Sci. doi:10.2205/2008ES000299

Bond G, Kromer B, Beer J, Muscheler R, Evans MN, Showers W, Hoffmann S et al (2001) Persistent solar influence on north Atlantic climate during the Holocene. Science 294(5549): 2130-2136. doi:10.1126/science.1065680

Bordi I, Fraedrich K, Sutera A (2009) Observed drought and wetness trends in Europe: an update. Hydrol Earth Syst Sci 13(8):1519-1530

Bouette JC, Chassagneux JF, Sibai D, Terron R, Charpentier A (2006) Wind in Ireland: long memory or seasonal effect? Stoch Environ Res Ris Assess 20(3):141-151

Broecker SW, Denton GH, Edwards RL, Cheng H, Alley RB, Putnam AE (2010) Putting the Younger Dryas cold event into context. Quat Sci Rev 29(9-10):1078-1081

Brohan P, Kennedy J, Harris I, Tett SFB, Jones P (2006) Uncertainty estimates in regional and global observed temperature changes: a new dataset from 1850. J Geophys Res. doi:10.1029/2005JD006548

Cook ER, Palmer JG and D'Arrigo RD (2002) Evidence for a ‘Medieval Warm Period’ in a 1,100 tree-ring reconstruction of past austral summer temperatures in New Zealand. Geophys Res Lett 29:1–4

Croll J (1864) On the physical cause of the change of climate during geological epochs. Philos Mag 28:121-137

Crowell JC, Frakes LA (1970) Phanerozoic glaciation and the causes of ice ages. Am J Science 268:193-224, doi:10.2475/ajs.268.3.193

Dansgaard W, GRIP Scientific Team (1993) Evidence for general instability in past climate from a 250-kyr ice-core record. Nat 364:218-220

Ditlevsen P (2009) Climate transitions on long timescales. Contemporary Phys 50(4):511-532

Drysdale RN, Hellstrom JC, Zanchetta G, Fallick AE, Sanchez Goni MF, Couchoud I, McDonald J, et al. (2009) Evidence for Obliquity Forcing of Glacial Termination II. Science 325(5947):1527-1531

Eichner JF, Koscielny-Bunde E, Bunde A, Havlin S and Schellnhuber H-J (2003) Power-law persistence and trends in the atmosphere: A detailed study of long temperature records. Phys Rev E, 68, 046133

Elkibbi M, Rial JA (2001) An outsider's review of the astronomical theory of the climate: is the eccentricity-driven insolation the main driver of the ice ages? Earth-Sci Rev 56(1-4):161-177

Ehsanzadeh E, Adamowski K. (2010) Trends in timing of low stream flows in Canada: impact of autocorrelation and long term persistence. Hydrol Process 24(8):970-980

Eltahir EAB (1996) El Niño and the Natural Variability in the Flow of the Nile River, Water Res Resour 32(1):131-137

Evans TE (1996) The effects of changes in the world hydrological cycle on availability of water resources. In: Global Climate Change and Agricultural Production: Direct and Indirect Effects of Changing Hydrological Pedological and Plant Physiological Processes, Chapter 2. FAO and John Wiley, Chichester, West Sussex, UK

Fraedrich K, Blender R (2003) Scaling of Atmosphere and Ocean Temperature Correlations in Observations and Climate Models. Phys Rev Lett 90(1-4):108501

Fraedrich K, Blender R, Zhu X (2009) Continuum climate variability: long-term memory, extremes, and predictability. Int J Mod Phys B 23 (28-29):5403-5416

Gama S, Ruskin H, Sharkasi A, Crane M, Matos (2008) Time and scale Hurst exponent analysis for financial markets. Phys A: Stat Mech Appl 387(15):3910-3915

Gies DR, Helsel JW (2005) Ice age epochs and Sun's path through the galaxy. Astrophys J 626:844–848

Gildor H, Tziperman E (2000) Sea ice as the glacial cycles climate switch: role of seasonal and orbital forcing. Paleoceanogr 15:605-615

Grove JM, Switsur (1994) Glacial geological evidence for the Medieval Warm Period. Clim Change 26:143–169

Hahn T, Dresler T, Ehlis A-C, Pyka M, Dieler AC, Saathoff C, et al (2012) Randomness of resting-state brain oscillations encodes Gray's personality trait. Neuroimage 16;59(2):1842-1845.

Haslett J, Raftery AE (1989) Space-Time Modelling with Long-Memory Dependence: Assessing Ireland's Wind Power Resource. J R Stat Soc 38(1):1-50

Hass H, Kuhn G, Forwick M, Vorren T (2008) The Medieval Warm Period and the Little Ice Age in marine sediments from Maxwell Bay, King George Island, West Antarctic Peninsula . The 33rd International Geological Congress, Oslo, Norway, August 6-14

Hasselmann K (1976) Stochastic Climate Models. 1. Theory. Tellus 28(6):473-485

Hurst HE (1951) Long term storage capacities of reservoirs. Trans Am Soc Civ Engr 116:776-808

Huybers P, Wunsch C (2005) Obliquity pacing of the late Pleistocene glacial terminations.

Nat 434(7032):491-494

Huybers P (2006) Early Pleistocene Glacial Cycles and the Integrated Summer Insolation Forcing. Science 313(5786):508-511

Huybers P (2007) Glacial variability over the last two million years: an extended depth derived age model, continuous obliquity pacing, and the Pleistocene progression. Quat Sci Rev 26(1-2):37-55

Huybers P, Tziperman E (2008) Integrated summer insolation forcing and 40,000 year glacial cycles: the perspective from an icesheet/energy-balance model. Paleoceanogr. doi:10.1029/2007PA001463

Huybers P (2009) Antarctica's Orbital Beat. Science 325(5944):1085–1086

Huybers P (2011) Combined obliquity and precession pacing of late Pleistocene deglaciations. Nat. doi:10.1038/nature10626

Imbrie J (1982) Astronomical theory of the Pleistocene ice ages: A brief historical review. Icarus 50(2-3):408-422

Imbrie J, Berger A, Kutzbach J, Pisias NG, Raymo ME, Shackleton NJ, et al. (1993) On the structure and origin of major glaciation cycles 2.The 100,000 year cycle. Paleocean 8: 699–735

Jiang T, Zhang Q, Blender R, Fraedrich K. (2005) Yangtze Delta floods and droughts of the last millennium: Abrupt changes and long term memory Theor Appl Climatol 82(3-4):131-141

Jouzel, J, EPICA Scientific Team (2007), EPICA Dome C Ice Core 800KYr Deuterium Data and Temperature Estimates, IGBP PAGES/World Data Center for Paleoclimatology. 2007-091NOAA/NCDC Paleoclimatology Program, Boulder Co

Karagiannis T, Molle M, Faloutsos M (2004) Long-Range Dependence: Ten Years of Internet Traffic Modeling. IEEE Internet Comp 8(5): 57-64

Kawamura K, Parrenin F, Lisiecki L, Uemura R, Vimeux F, Severinghaus JP, Hutterli MA, et al. (2007) Northern Hemisphere forcing of climatic cycles in Antarctica over the past 360,000 years. Nat 448(7156):912–916

Khaliq MN, Gachon P. Pacific Decadal Oscillation Climate Variability and Temporal Pattern of Winter Flows in Northwestern North America (2010) J Hydrometeor 11(4):917-933

Kirkby J (2007) Cosmic rays and climate. Surv Geoph 28:333-375

Klemes V (1974) The Hurst phenomenon: A puzzle? Water Resour Res 10(4):675-688

Kolmogorov AN (1940) Wienersche Spiralen und einige andere interessante Kurven in Hilbertschen Raum. Dokl Akad Nauk URSS 26:115-118

Kominz, MA, Pisias NG (1979) Pleistocene climate: Deterministic or stochastic? Science 204:171-173

Koscielny-Bunde E, Bunde A, Havlin S, Roman HE, Goldreich Y, Schellnhuber HJ (1998) Indication of a universal persistence law governing atmospheric variability. Phys Rev Lett 81:729-732

Koutsoyiannis D (2002) The Hurst phenomenon and fractional Gaussian noise made easy. Hydrol Sci J 47(4):573-595

Koutsoyiannis D (2003a) Climate change, the Hurst phenomenon, and hydrological statistics. Hydrol Sci J 48(1):3-24

Koutsoyiannis, D. (2003b), Hydrological statistics for engineering design in a varying climate, EGS-AGU-EUG Joint Assembly, Geophysical Research Abstracts, Vol. 5, Nice, April 2003, European Geophysical Society, American Geophysical Union (http://www.itia.ntua.gr/g/docinfo/565/)

Koutsoyiannis D (2010) A random walk on water. Hydrol. Earth Syst Sci, 14:585–601

Koutsoyiannis D (2011a) Hurst-Kolmogorov dynamics as a result of extremal entropy production. Physica A 390(8):1424–1432

Koutsoyiannis D (2011b) Hurst-Kolmogorov dynamics and uncertainty. J American Water Resour Assoc 47(3):481–495

Koutsoyiannis D, Montanari A (2007) Statistical analysis of hydroclimatic time series: Uncertainty and insights. Water Resour Res 43 (5):W05429, doi:10.1029/2006WR005592

Koutsoyiannis D, Cohn TA (2008) Hurst-Kolmogorov pragmaticity and climate. Climatic and hydrological perspectives on long-term changes, European Geosciences Union General Assembly. (Available in http://itia.ntua.gr/getfile/849/2/documents/2008EGU_HurstClimatePr.pdf)

Koutsoyiannis D, Montanari A, Lins HF, Cohn TA (2009) Climate, hydrology and freshwater: towards an interactive incorporation of hydrological experience into climate research—DISCUSSION of "The implications of projected climate change for freshwater resources and their management". Hydrol Sci J, 54(2):394–405

Lasdon, L.S., Smith, S., 1992. Solving sparse nonlinear programs using GRG. ORSA Journal on Computing 4 (1), 2–15.

Lasdon, L.S., Waren, A., Jain, A., Ratner, M., 1978. Design and testing of a generalized reduced gradient code for nonlinear programming. ACM Transactions on Mathematical Software 4 (1), 34–50.

Laskar J, Robutel P, Joutel, F, Gastineau M, Correia ACM, Levrard B (2004) A long term numerical solution for the insolation quantities of the Earth. Astron Astrophys. doi: 10.1051/0004-6361:20041335

Deleted: ¶

Deleted: Koutsoyiannis D, Montanari A. (2007) Statistical analysis of hydroclimatic time series:

Lai MC, Lombardo MV, Chakrabarti B, Sadek SA, Pasco G, Wheelwright SJ, Bullmore ET, Baron-Cohen S, MRC AIMS Consortium, Suckling J (2010) A Shift to Randomness of Brain Oscillations in People with Autism. Biol Psyc. doi:10.1016/j.biopsych.2010.06.027

Leland WE, MS Taqqu, W Willingerand, Wilson DV (1994) On the self-similar nature of Ethernet traffic (extended version). IEEE/ACM Trans Netw 2(1):1-15

Leland WE, MS Taqqu, W Willingerand, Wilson DV (1995) On the self-similar nature of Ethernet traffic. ACM SIGCOMM Comput Commun Rev 25(1):202—213

Lennartz S, Bunde A (2011) Distribution of natural trends in long-term correlated records: A scaling approach. Phys Rev E 84(2):021129

Lin LY, Lin JL, Du CC, Lai LP, Tseng YZ, Huang SKS (2001) Reversal of deteriorated fractal behavior of heart rate variability by beta-blocker therapy in patients with advanced congestive heart failure. J Cardiovasc Electrophysiol 12(1):26-32

Lisiecki LE, Raymo ME (2005) A Pliocene-Pleistocene stack of 57 globally distributed benthic d18O records. Paleoceanogr. doi:10.1029/2004PA001071.

Liu Z, Cleveland L, Herbert T (2007) Early onset and origin of 100-kyr cycles in Pleistocene tropical SST records. Earth Planet Sci Lett 265:703-715

Liu H-S, & Chao BF (1998). Wavelet Spectral Analysis of the Earth's Orbital Variations and Paleoclimatic Cycles. J Atmos Sci, 55(2), 227–236

Lo A (1991) Long term memory in stock market prices. Econometrica 59:1279–1313

Maurizio S, Molnar P, Burlando P (2011) Seasonal long-term persistence in radar precipitation in complex terrain. Water Resour Res. doi:10.1029/2010WR010170

Lohle C (2007) A 2000-year global temperature reconstruction based on non-treering proxies. Energy Environ 18(7-8):1049-1058

Long M, Jinghlu W, Hong Y, Haiao Z, Abuduwaili J (2011) The Medieval Warm Period and the Little Ice Age from a sediment record of Lake Ebinur, northwest China. Boreas 40:518–524

Lourens LJ, Becker J, Bintanja R, Hilgen FJ, Tuenter E, van de Wal RS, Ziegler M (2010) Linear and non-linear response of late Neogene glacial cycles to obliquity forcing and implications for the Milankovitch theory. Quat Sci Rev 29(1-2):352-365

Maxim V, Sendur L, Fadili J, Suckling J, Gould R, Howard R, Bullmore E (2005) Fractional Gaussian noise, functional MRI and Alzheimer's disease. NeuroImage 25:141–158

Mandelbrot BB, Wallis JR (1968) Noah, Joseph, and operational hydrology. Water Resour Res 4(5):909-918

Mangerud J, Gulliksen S and Larsen E (2010) 14C-dated fluctuations of the western flank of the Scandinavian Ice Sheet 45–25 kyr BP compared with Bølling–Younger Dryas fluctuations and Dansgaard–Oeschger events in Greenland. Boreas 39:328–342

Mesa O and Poveda G (1993) The Hurst Effect: The scale of fluctuation approach. Water Resour Res 29(12):3995:4002

Milankovitch M (1941) Kanon der Erdbestrahlung und seine Andwendung auf das Eiszeitenproblem. Royal Serbian Academy Special Publication,133, Belgrade [English version published by the Israel Program for Scientific Translations, Jerusalem, 1969.]

Moberg A, Sonechkin D, Holmgren K, Datsenko N, Karlén W (2005), Highly variable Northern Hemisphere temperatures reconstructed from low- and high-resolution proxy data. Nat 433(7026):613-617

Montanari A, Rosso R, Taqqu MS (1997) Fractionally differenced ARIMA models applied to hvdrologic time series. Wat Resour Res 33(5):1035-1044

Mukhopadhyay B, Acharyya A, Dasgupta S (2008) Statistical analysis on yearly seismic moment release data to demarcate the source zone for an impending earthquake in the Himalaya. Acta Geophys 57(2):387-399

Muller RA, MacDonald GJ (2000) Ice ages and astronomical causes. Springer Praxis, Chichester, UK

Naish T, Powell R, Levy R, Wilson G et al. (2009) Obliquity-paced Pliocene West Antarctic ice sheet oscillations. Nat 458(7236):322-328

Navarro X,Beuchee A, Poree F, Carrault G (2011) Performance analysis of Hurst's exponent estimators in higly immature breathing patterns of preterm infants. Proceedings of IEEE International Conference on Acoustics, Speech and Signal Processing (ICASSP), doi: 10.1109/ICASSP.2011.5946500

Norouzzadeh P, Dullaert W, Rahmani B (2007) Anti-correlation and multifractal features of Spain electricity spot market. Phys A: Stat Mech Appl 380:333-342

Padmanabhan G, Shrestha SL, Kavasseri RG (2008) Persistence in North American Palmer drought severity index data reconstructed from tree ring history. Poster presentation in 13th World Water Congress, Montpellier, France

Paillard D (1998) The timing of Pleistocene glaciations from a simple multiple-state climate model. Nat 391(6665):378-381

Paillard D (2010) Climate and the orbital parameters of the Earth. Comptes Rendus Geoscience 342(4-5):273-285

Pelletier J (1997) Analysis and Modeling of the Natural Variability of Climate. J Clim 10(6):1331-1342

Pelletier J (2003) Coherence resonance and ice ages. J Geophys Res. doi:10.1029/2002JD003120

Peng CK, Buldyrev SV, Havlin S, Simons M, Stanley HE, Goldberger AL (1994) Mosaic organization of DNA nucleotides. Phys Rev E 49(2):1685-1689

Pettersen EL, Larsen SE (1978) Statistical study of a composite isotopic, paleotemperature series from the last 700,000 years. Tellus 30:193-200

Pisias NG, Moore TC (1981) The evolution of Pleistocene climate: a time series approach. Earth Planet Sci Lett 52:450-458

Pollack HN, Smerdon JE (2004) Borehole climate reconstructions: spatial structure and hemispheric averages. J Geophys Res 109. doi:10.1029/2003JD004163

Radziejewski M, Kundzewicz ZW (1997) Fractal analysis of flow of the river Warta. J Hydrol 200:280–294

Rahmstorf S et al (2004) Cosmic rays, carbon dioxide, and climate. Eos 85(4):38–40

Ramachandra Rao A, Azli M, Pae LJ (2011) Identification of trends in Malaysian monthly runoff under the scaling hypothesis. Hydrol Sci J 56(6):917-929

Rasouli G, Rasouli M, Lenz FA, Verhagen L, Borrett DS, Kwan HC (2006) Fractal characteristics of human Parkinsonian neuronal spike trains. Neurosci 139(3):1153-1158

Rial JA (1999) Pacemaking the Ice Ages by Frequency Modulation of Earth's Orbital Eccentricity. Science 285(5427):564-568

Richards GR (1994) Orbital forcing and endogenous interactions: Non-linearity, persistence and convergence in late Pleistocene climate. Quat Sci Rev 13(8):709-725

Riemann-Campe K, Blender R, Fraedrich K (2011) Global memory analysis in observed and simulated CAPE and CIN. Int J Climatol 31(8):1099-1107

Roe G (2006) In defense of Milankovitch, Geophys Res Lett. doi:10.1029/2006GL027817

Royer DL et al (2004) CO2 as a primary driver of Phanerozoic climate. GSA Today 14(3):4–10

Rybski D, Bunde A, Havlin S, von Storch H (2006) Long-term persistence in climate and the detection

problem. Geophys Res Lett. doi:10.1029/2005GL025591

Saltzman B (1982) Stochastically-driven climatic fluctuations in the sea-ice, ocean temperature, CO2, feedback system. Tellus 34:97–112

Sakalauskiene G (2003) The Hurst Phenomenon in Hydrology. Environ Res, Eng Manag 3(25):16-20

Serinaldi F (2010) Use and misuse of some Hurst parameter estimators applied to stationary and non-stationary financial time series. Phys A: Stat Mech Appl 389(14):2770-2781

Serletis A, Rosenberg AA (2007) The Hurst exponent in energy futures prices. Phys A 380:325–332

Shackleton NJ, Imbrie J (1990) The δ18O spectrum of oceanic deep water over a five-decade band. Clim Change 16(2):217-230. doi: 10.1007/BF00134658

Shaviv NJ, Veizer J (2003) Celestial driver of Phanerozoic climate? GSA Today, Geol Soc Am 4–10

Sheng H, Chen YQ, Qiu T (2011) Heavy-tailed distribution and local long memory in time series of molecular motion on the cell membrane. Fluc Noise Lett 10(01):93

Stanley HE, Afanasyev V, Amara LAN, Buldyrev SV, Goldberger AL, Havlin S, Leschhorn H, Maass P, Mantegna RN, Peng CK, Prince PA, Salinger MA, Stanley MHR, Viswanathan GM (1996) Anomalous fluctuations in the dynamics of complex systems: from DNA and physiology to econophysics. Phys A: Stat Mech Appl;224(1-2):302-321.

Steig EJ, Morse DL, Waddington ED, Stuiver M, Grootes PM., Mayewski PA, Twickler MS, Whitlow SI (2000) Wisconsinan and Holocene climate history from an ice core at Taylor Dome, Western Ross Embayment, Antarctica. Geografiska Annaler: Series A, Phys Geogr 82(2-3):213–235

Stephenson DB, Paven P, Bojariu R (2000) Is the North Atlantic Oscillation a random walk? Int J Climatol 20:1–18

Suwa M, Bender ML (2008) Chronology of the Vostok ice core constrained by O2/N2 ratios of occluded air, and its implication for the Vostok climate records. Quat Sci Rev 27:11-12

Telesca L, Cuomo V, Lapenna V, Vallianatos F (2000) Self-similarity properties of seismicity in the Southern Aegean area. Tectonophys 321(1):179-188

Tziperman E, Raymo M, Huybers P, Wunsch C (2006) Consequences of pacing the Pleistocene 100 kyr ice ages by nonlinear phase locking to Milankovitch forcing. Paleoceanogr. doi:10.1029/2005PA001241.

Wallmann K (2004) Impact of atmospheric CO2 and galactic cosmic radiation on Phanerozoic climate change and the marine d18O record. Geochemistry Geophysics Geosystems 5.

Deleted: Steig EJ, Morse DL, Waddington ED, Stuiver M, Grootes PM, Mayewski PA, Twickler MS,

doi:10.1029/2003GC000683

Wang G, Jiang T, Chen G (2006) Structure and long-term memory of discharge series in Yangtze River. Acta Geogr Sinica 61(1):47-56

Whitlow SI (2000) Wisconsinan and Holocene climate history from an ice core at Taylor Dome. Phys Geogr 82:213-235

Winograd IJ, Coplen TB, Landwehr JM, Riggs AC, Ludwig KR, Szabo BJ, Kolesar PT, et al. (1992) Continuous 500,000-Year Climate Record from Vein Calcite in Devils Hole, Nevada. Science 258(5080):255-260

Wunsch C (2004) Quantitative estimate of the Milankovitch-forced contribution to observed Quaternary climate change. Quat Sci Rev 23:1001–1012

Yano J, Blender R, Zhang C, Fraedrich K (2004) 1/f - Noise and pulse-like events in the tropical atmospheric surface variabilities. Q J R Meterol Soc 130:1697-1721

Varotsos C, Kirk-Davidoff D (2006) Long-memory processes in ozone and temperature variations at the region 60° S–60° N. Atmos Chem Phys 6(12):4093-4100

Veizer J, Ala D, Azmy K, Bruckschen P, Buhl D, Bruhn F, Carden GAF, Diener A, Ebneth S, Godderis Y, Jasper T, Korte C, Pawellek F, Podlaha O, Strauss H (2000) 87Sr/86Sr, d13C and d18O evolution of Phanerozoic seawater. Chem Geol 161:59-88

Zachos J, Pagani M, Sloan L, Thomas E, Billups K (2001) Trends, rhythms, and aberrations in global climate 65 Ma to present. Science 292(5517):686-693

Table 1. Instrumental and proxy time series of global temperature used in the study.

Abbre-viation	Type of data (unit)	Total length, L (years)	Original resolution range (years)**	Regularized resolution, Δ (years)	Reference	Data availability from
NSSTC	Satellite (^{o}C)	32	1/12	1/12		www.nsstc.uah.edu/ data/msu/t2lt/
CRU	Instrumental (^{o}C) (weather stations)	161	1/12	1/12	Brohan et al. (2006)	www.cru.uea.ac.uk/cru/data/temperature/
Moberg	Multi-proxy (^{o}C)	2×10^{3}	1	1	Moberg (2005)	www.ncdc.noaa.gov/paleo/pubs/moberg2005/moberg2005.html
Lohle	Multi-proxy (^{o}C)	2×10^{3}	1	30*	Lohle (2007)	www.ncasi.org/programs/areas/climate/LoehleE&E2007.csv
Taylor	Single-proxy ice core (δ^{18}O)	10×10^{3}	1.4–96.1	100	Steig et al. (1999)	ftp://ftp.ncdc.noaa.gov/pub/data/paleo/icecore/antarctica/taylor/hi18o_td.t
GRIP	Single-proxy ice core (δ^{18}O)	100×10^{3}	0.9–172 (3.6%)	100	Dansgaard et al. (1993)	www.ncdc.noaa.gov/paleo/icecore/greenland/summit/document/gripisot.htm
EPICA	Single-proxy ice core (^{o}C)	800×10^{3}	8.2–1364 (6.4%)	500	Jouzel et al. (2007)	www.ncdc.noaa.gov/paleo/pubs/jouzel2007/jouzel2007.html
Huybers	Multi-proxy sediment (δ^{18}O)	2.6×10^{6}	10^{3}	10^{3}	Huybers (2007)	www.people.fas.harvard.edu/~phuybers/Progression/Averages.txt
Lisiecki - Raymo	Multi-proxy sediment (δ^{18}O)	3×10^{6}	$1–2.5\times10^{3}$	2.5×10^{3}	Lisiecki and Raymo (2005)	http://lorraine-lisiecki.com/LR04stack.txt
Zachos	Multi-proxy sediment (δ^{18}O)	60×10^{6}	$1–120\times10^{3}$ (0.4%)	50×10^{3}	Zachos et al. (2001)	www.ncdc.noaa.gov/paleo/metadata/noaa-ocean-8674.html
Veizer	Multi-proxy sediment (^{o}C)	480×10^{6}	2–16 050×10^{3}*** (1.1%)	500×10^{3}	Veizer et al. (2000)	mysite.science.uottawa.ca/jveizer/isotope_data/index.html

*Scales of 1 to 30 years were not included because the series is smoothed by Lohle (2007) at the 30-year scale.

** In parenthesis the percent of time steps of the original series that are greater than the chosen regularized resolution, Δ.

*** This high value results from a single large gap in the series.

Deleted: nsidc.org/data/docs/agdc/nsidc0315_ahn/index.html

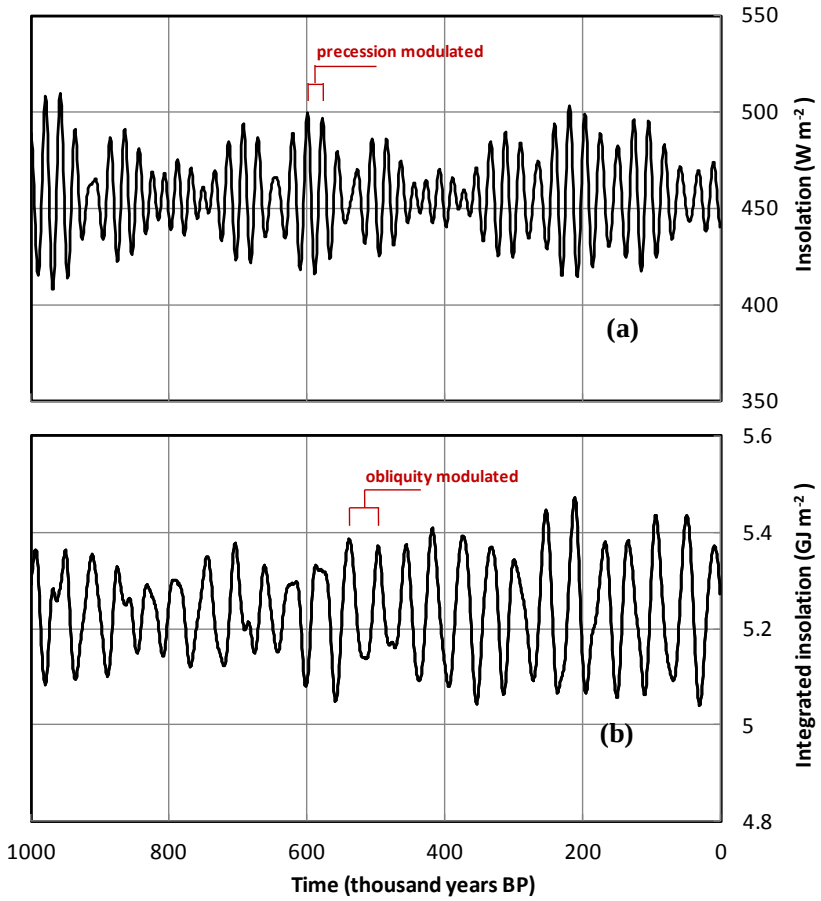

Fig. 1 Summer insolation at 65°N: (a) on the day of summer solstice, and (b) integrated over summer. Series (a), calculated by Laskar et al. (2004) and corresponding to Milankovitch' insolation, shows 19–24 thousand-year periodicities and is precession-dependent, whereas in series (b), calculated by Huybers (2006), the periodicity shifts to 41 thousand years, thus reflecting the obliquity band.

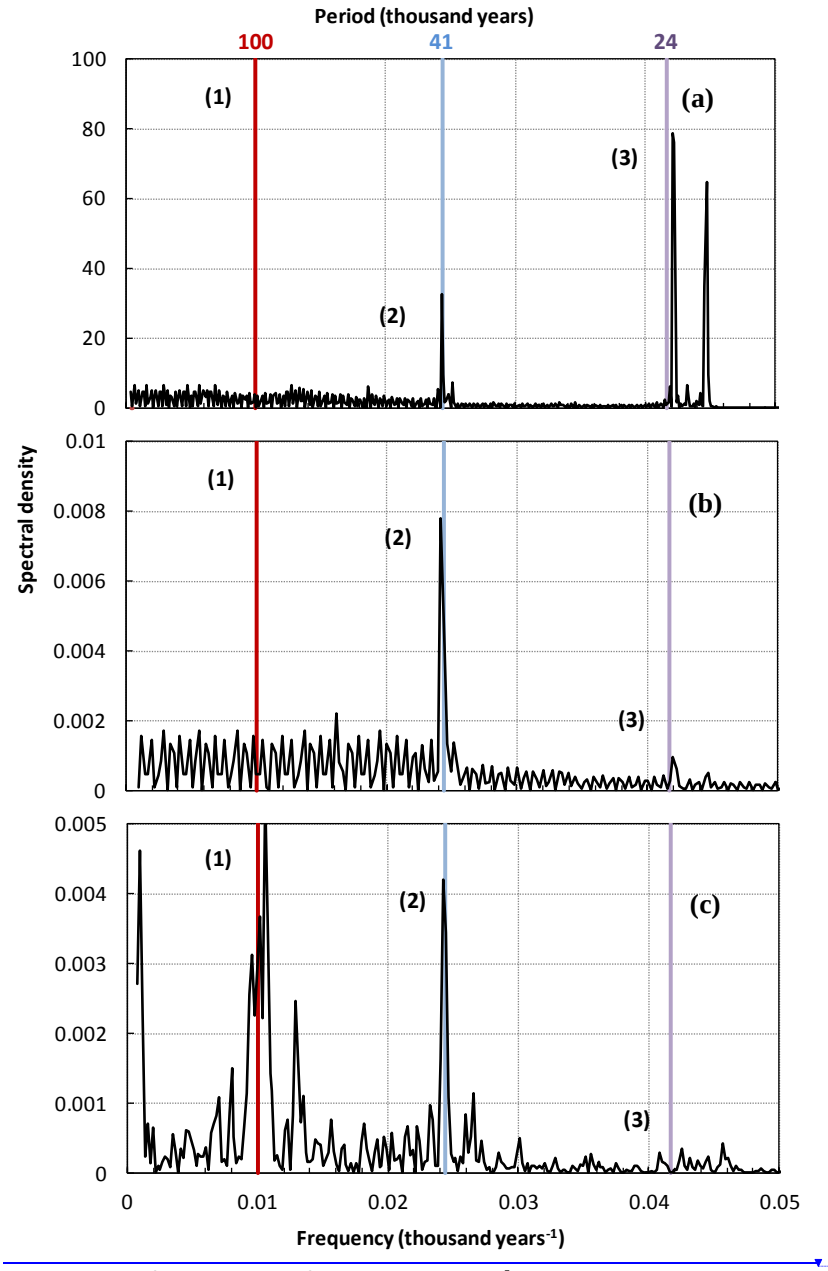

Fig. 2 Power spectra of: (a) insolation forcing in June at 65°N (classical orbital theory; Laskar et al. 2004), (b) integrated summer insolation at 65°N (modern orbital theory; Huybers 2006), and (c) two-million year temperature reconstruction (Huybers 2007). In (a) the obliquity cycle at 41 thousand years (marked as 2), and the precession cycles at 19 and 24 thousand years (marked as 3) have similar amplitude, whereas in (b) only the obliquity constituent is dominant. The power spectrum of temperature reconstruction (c) agrees with (b) and (c) in terms of the obliquity cycle, while it contains an additional peak at 100 thousand years (marked as 1) which does not appear in (a) or (b).

Deleted:

Deleted: 1

Deleted: 2

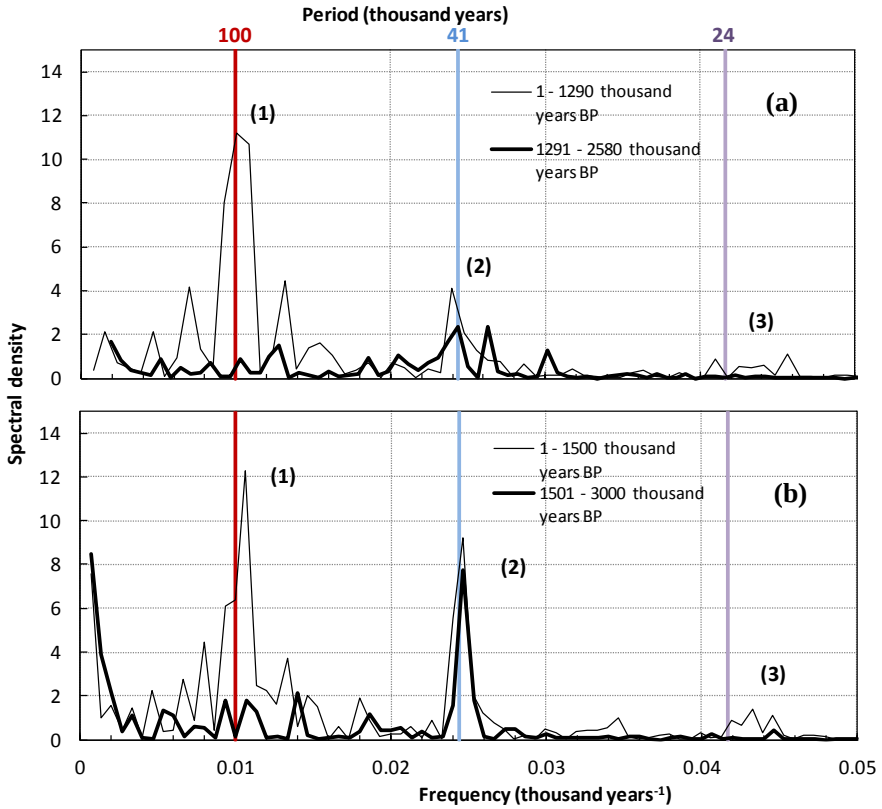

Fig. 3 Spectral analysis of the temperature reconstructions by (a) Huybers (2007) and (b) Lisiecki and Raymo (2005). Each of the reconstructions was split into two equal parts, and their power spectra were calculated separately. The eccentricity signal (marked as 1) appears strong in the first part of both reconstructions (a) and (b), but disappears in the second; the obliquity signal (marked as 2) is strong in each part of reconstruction (b); precession (marked as 3) is very weak in all cases.

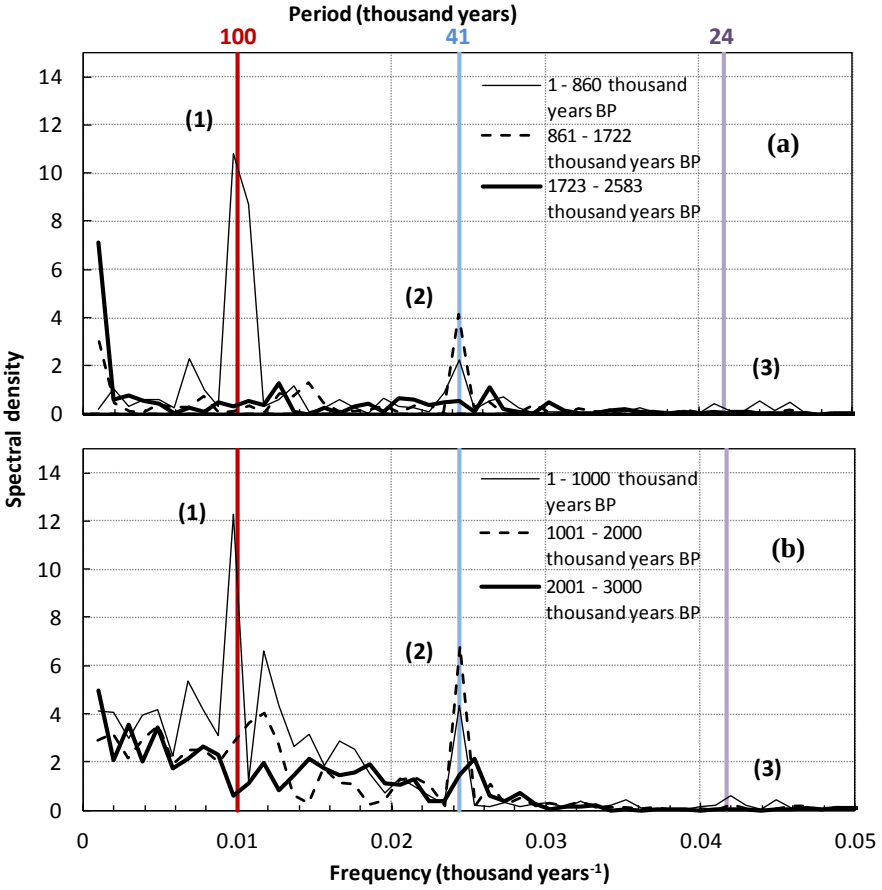

Fig. 4 Spectral analysis of the temperature reconstructions by (a) Huybers (2007) and (b) Lisiecki and Raymo (2005), as in Figure 3 except that each of the reconstructions was split into three equal parts.

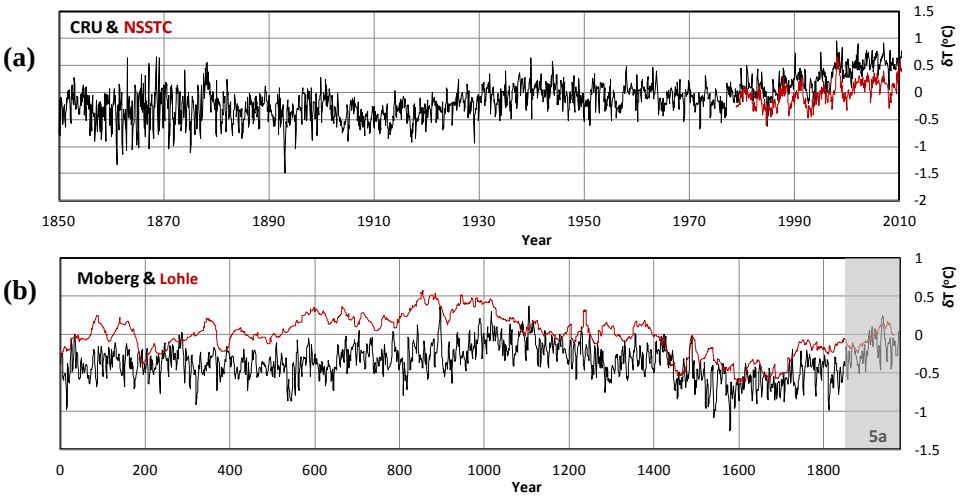

Fig. 5 Global temperature series of: (a) instrumental data going back to 32 and 160 years, respectively, and (b) multi-proxy reconstructions going back up to 2000 years (see Table 1). The gray area indicates the link of the time period of the series with the one before it.

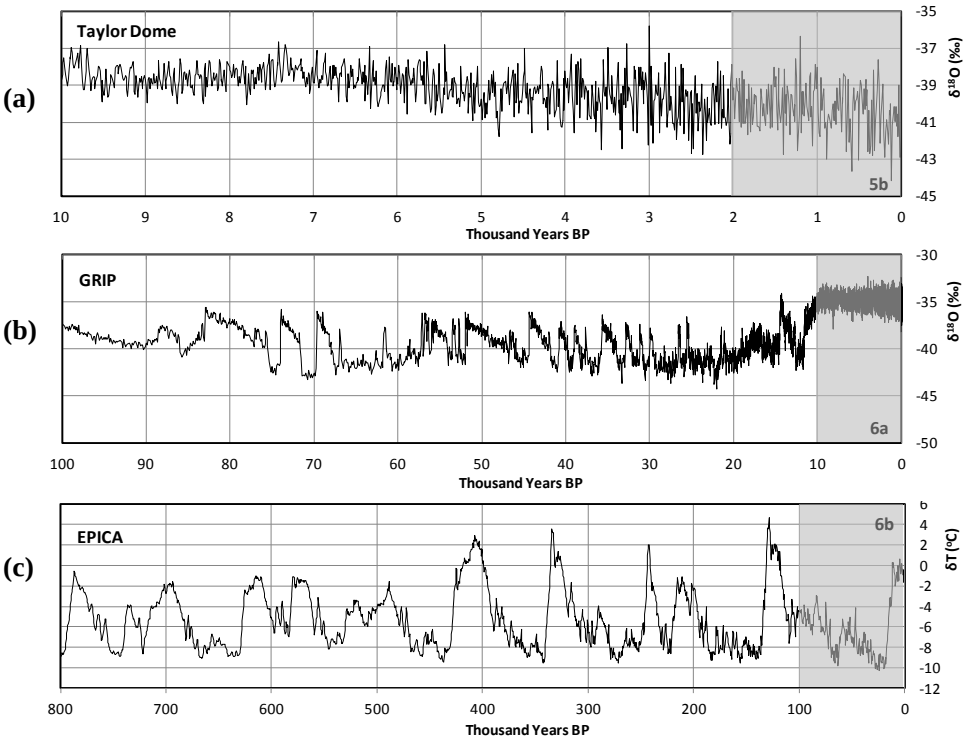

Fig. 6 Global temperature series from ice core reconstructions going back up to about 800 thousand years BP (see Table 1). The gray areas provide the links of the time period of each series with the one before it (with Figure 5(b) for (a)).

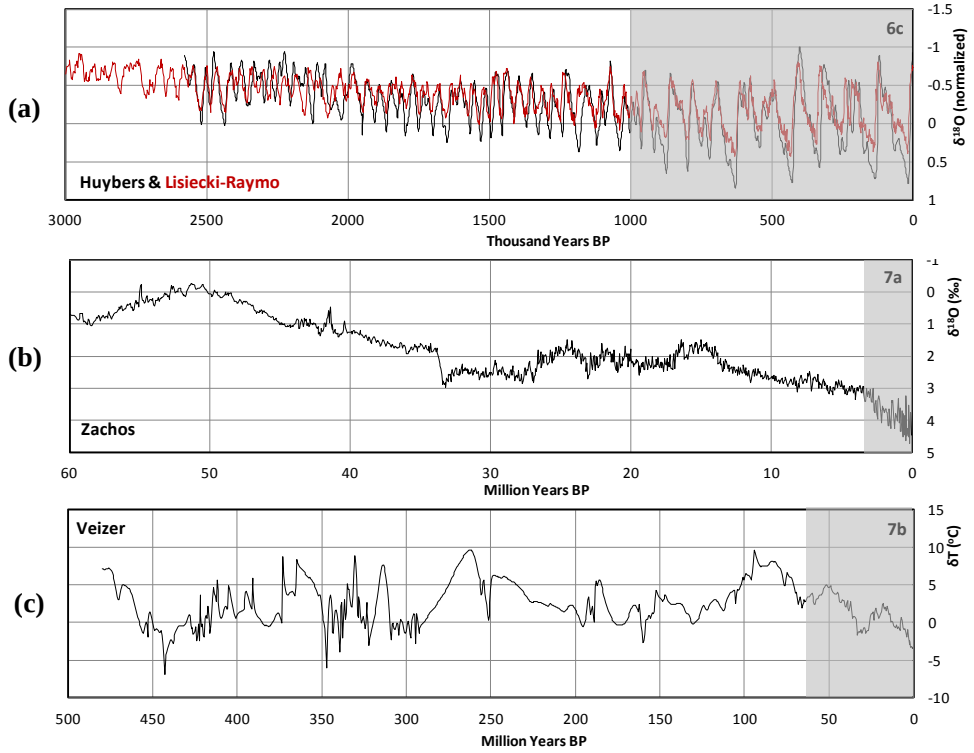

Fig. 7 Global temperature series from sediment reconstructions going back up to about 500 million years BP (see Table 1). The gray areas indicates the links of the time period of each series with the one before it (with Figure 6(c) for (a)).

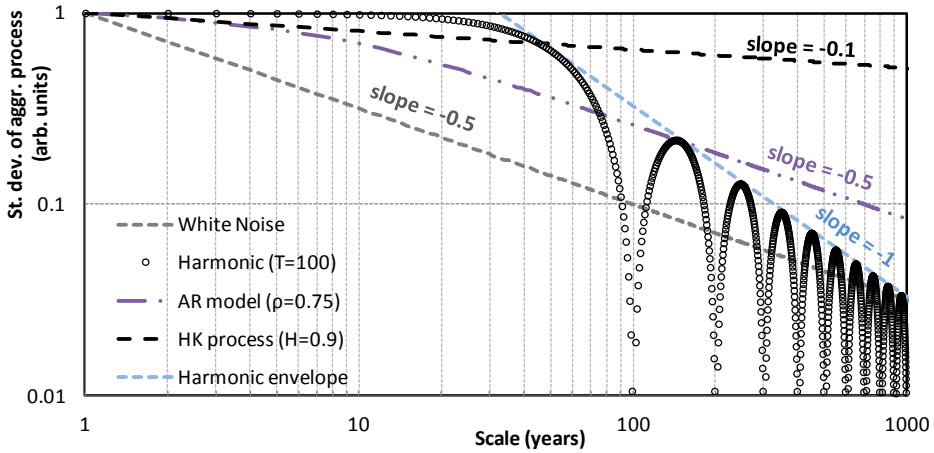

Fig. 8 Climacograms for: (a) a white noise (purely random) process, (b) a purely periodic process with period 100, (c) an AR(1) (Markov) process with $\rho = 0.75$, and (d) an HK process with $H = 0.9$.

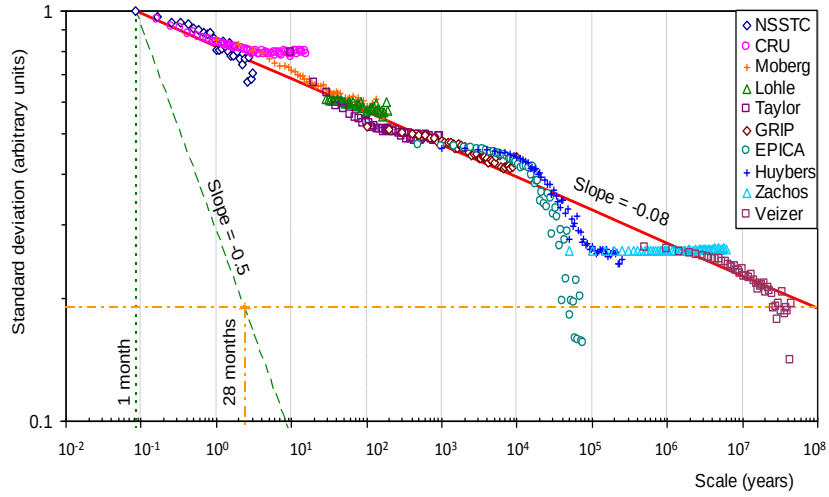

Fig. 9 Combined climacogram of the ten temperature observation series and proxies. The dotted line with slope –0.5 represents the climacogram of a purely random process. The horizontal dashed-dotted line represents the climatic variability at 100 million years, while the vertical dashed-dotted line at 28 months, represents the corresponding scale to the 100-million-year variability if climate was random (classical statistics approach). For explanation about the groups of points departing from the solid straight line (with slope -0.08) see Fig. 10 and its description in text.

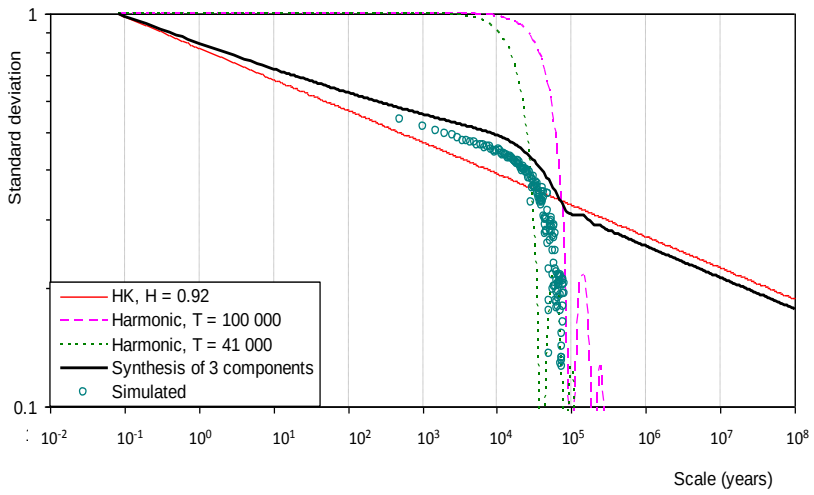

Fig. 10 Theoretical climacograms of an HK process with H = 0.92 and two periodic processes with periods 100 and 41 thousand years, all having unit standard deviation at monthly scale, along with the climacogram of the synthesis (weighted sum) of these three components with weights 0.95, 0.30 and 0.15, respectively; the empirical climacogram of a time series simulated from the synthesis process with time step and length equal to those of the EPICA series is also plotted.

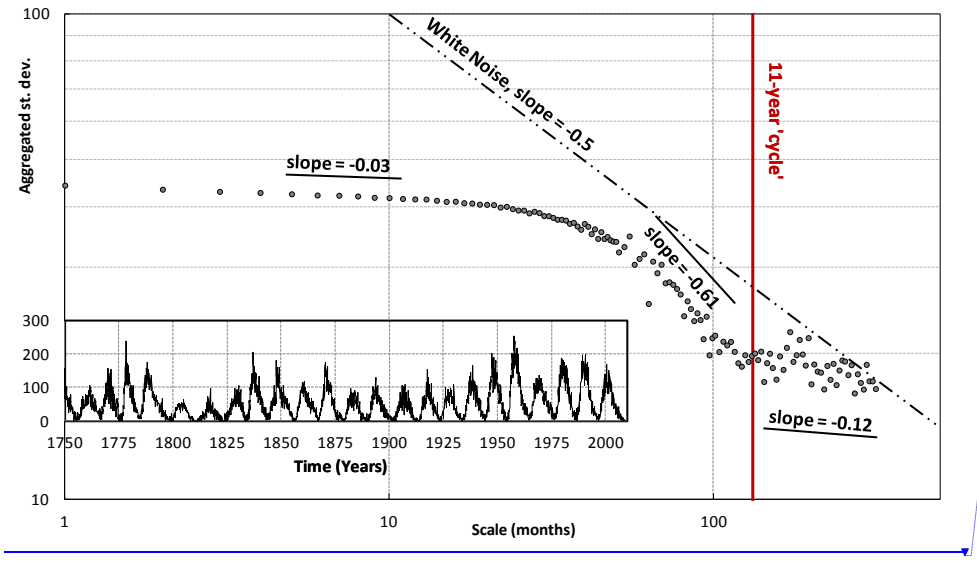

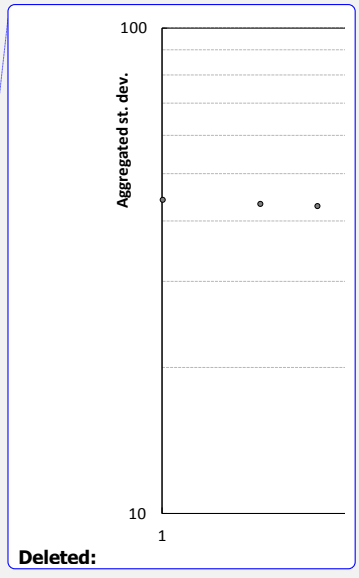

Fig. 11 Climacogram of sunspot number from original data (shown in the embedded graph) from the Royal Greenwich Observatory & USAF/NOAA (http://solarscience.msfc.nasa.gov/greenwch/spot_num.txt).